Doping of Titanium Dioxide with Zirconia for Application of Dye Sensitized Solar Cell

by

SYAZWAN B. ABD RAHMAN

Dissertation submitted in partial fulfilment of

the requirements for the

Bachelor of Engineering (Hons)

(Chemical Engineering)

JANUARY 2010

Universiti Teknologi PETRONAS

Bandar Seri Iskandar

31750 Tronoh

Perak Darul Ridzuan

CERTIFICATION OF APPROVAL

Doping of Titanium Dioxide with Zirconia for Application of Dye Sensitized Solar Cell

by

SYAZWAN B. ABD. RAHMAN

A project dissertation submitted to the
Chemical Engineering Programme
Universiti Teknologi PETRONAS
in partial fulfilment of the requirement for the
BACHELOR OF ENGINEERING (Hons)
(CHEMICAL ENGINEERING)

Approved by,

_____

(AP. DR. ANITA BT RAMLI)

UNIVERSITI TEKNOLOGI PETRONAS
TRONOH, PERAK
January 2010

CERTIFICATION OF ORIGINALITY

This is to certify that I am responsible for the work submitted in this project, that the original work is my own except as specified in the references and acknowledgements, and that the original work contained herein have not been undertaken or done by unspecified sources or persons.

_____

SYAZWAN B ABD. RAHMAN

ABSTRACT

The study on the effect of doping TiO_2 with Zirconia was done by using Reflux and Impregnation synthesis method. The initial molar composition of Zr/TiO_2 was prepared at 1:1, 1:0.5 and 0.5:1 ratio. The produced samples from synthesis method then dried and calcined at 600^oC. The effect of varied composition was determined by characterization techniques as discussed in Chapter 4. The characterization techniques include XRD analysis, SEM analysis, BET analysis, FTIR analysis, Raman Spectroscopy analysis, XPS analysis and application on test cell.

Images from SEM analysis shown that more uniform distribution of nanoparticles, with reducing pore size and smaller grain size for samples with higher content of Zirconia. XRD and Raman analysis indicated the wide distribution of the monoclinic ZrO and tetragonal TiO_2 anatase phase. Higher content of Titania in the samples yield worse ceramic sinterability. FTIR result shown the reduction of hydroxyl and N-H group for the samples that has been calcined.

ACKNOWLEDGEMENT

I would like to express deepest gratitude to the Chemical Engineering Department of Universiti Teknologi PETRONAS (UTP) for providing me this chance to undertake this remarkable Final Year Project. It is a great challenge for me since I am not very familiar with this topic, but since the topic is interesting and I am willing to improve my knowledge, I am able to complete this study.

A very special note of thanks and appreciation to AP. Dr. Anita Ramli, my beloved Project Supervisor, who was always willing to assist me and provided good support throughout. Your excellent support, patience and effective guidance have helped my project to completion.

I would like to thank the Final Year Project committees, especially Dr. Khalik for arranging various seminars and useful briefing as support and knowledge to assist the student in the project. The seminars were indeed very helpful and insightful to us. I would like to thank all lecturers from Universiti Teknologi PETRONAS who had given me guidance throughout the period of the project. Not to be forgotten, the technicians in Chemical and Mechanical Department who always willing to assist me despite the equipment limitation and time constraint.

Last but not least, my heartfelt gratitude goes to my family and friends for providing me continuous support throughout the duration of this project.

Table of Contents

List of Figures

List of Tables

CHAPTER 1

INTRODUCTION

1.1 BACKGROUND OF STUDY

A dye sensitized solar cell is relatively new class of low cost solar cells. It is based on a semiconductor formed between the photo-sensitized anode and electrolyte, a photo electrochemical system. This cell was invented by Michael Gratzel and Brian O'Regan at the École Polytechnique Fédérale de Lausanne in 1991 and are also known as Grätzel cells (O' Regan and Gratzel, 1991).

The application of DSSC is extremely promising since it is made from low cost material and it does not need additional apparatus in its construction. If the DSSC is manufactured in bulk, the cost will be significantly lower than the previous silicon solar cell. DSSC can be engineered into a flexible sheet and also mechanically robust. Eventhough the conversion efficiency to electricity is lower compared to silicon solar cell, but if compare to performance-value ratio, DSSC shows great capability as new alternative to the power sources.

One of main component in the DSSC is nanoparticles, which is Titanium Dioxide (TiO_2). TiO_2 has been widely used as photocatalyst in solar energy conversion and environmental application because of relatively high activity, chemical stability, low cost and non-toxic (Baochao et al., 2008). But, the main problem associated with the usage of TiO_2 is slower reaction rate and also poor solar efficiency. The problems hinder further application of DSSC in industry.

A lot of research has been made in order to improve the efficiency of DDSC. Modifications on the component involved in DSSC such as electrolyte, nanoparticles, or dye and a lot more on many variables have been made to achieve better result. For

examples, the method was by establishing the junction between titania and other semiconductors; like doping titania with metal, ions, or composite design with porous materials. The synthesis method of producing Zirconia-Titania also plays major part in effectiveness of electricity conversion. The synthesis method may include sol-gel, polymer gel templating, homogeneous co-precipitation, hydrothermal, reflux or impregnation techniques (Baochao et al., 2008).

The focus of this project is to study the influence of metal doping in TiO_2. The metal compound selected for this study is Zirconia. Zirconia has been selected as the testing material for the nanoparticles in this study. Zirconia ceramics has been tested and proven to have good catalytic properties, thermodynamically stable and have excellent dielectric properties (Ussui, 2003). The synthesis method selected for the study is impregnation and reflux method.

Throughout this study, we will be able to analyze whether practice of doping Titanium Dioxide with Zirconia are able to broaden the band range gap of the light that can be absorbed by the dye sensitized cells so that it will has wider spectrum frequency response. In the end of the project, we can verify whether it is efficient to the low frequency range of visible light. At the same time, the project should be able improve the efficiency by increasing the conversion of photon into electron. The solar cells must also have long lifespan with little efficiency degradation.

1.2 PROBLEM STATEMENT

TiO_2 was sensitive and only limited to high-end solar spectrum, in the UV and blue light. TiO_2 did not give proper frequency in low end solar spectrum, which is in red light and visible light. The study was to improve the conversion efficiency of solar light in visible light to electricity.

1.3 OBJECTIVE OF STUDY

The objective of the project is based on the development and characterization of using TiO_2 doped with Zirconia as new alternative of nanoparticles in DSSC.

1) To synthesize Zr/TiO_2 from two synthesis methods which are reflux and impregnation methods. The effect of varied initial molar ratio (Zr/TiO_2: 1:1, 1:0.5, 0.5:1) was also analyzed in the study. Based on the characterization result, the best synthesis techniques and initial component content will be discussed.
2) To characterize the produce Zr/TiO_2 nanoparticles from the experimental procedures. The characterization will include test and analysis on the physical structural of the compound, stability, heat thermal, photocatalyst and diaelectric properties that will be discussed further in Result and Discussion section.
3) To incorporate the synthesized nanoparticles into a test cell and test the electricity generated.

1.4 SCOPE OF STUDY

The scope of study covered the various techniques of synthesization of Zirconium Titanate and method of characterization. The synthesize technique includes preparation by reflux and impregnation. The previous researches and studies related to those techniques will be studied for further understanding. The influence of varied initial component composition was studied. Next, the product from the synthesis will be characterized. The characterization technique will include XRD analysis, SEM analysis, BET analysis and other analyses techniques that will be discussed further in Methodology section. After analyzing each of the products from synthesis route option, selection will be made for the best synthesis technique for Zr/TiO_2 nanoparticles. The synthesized nanoparticles will be used in application of test cell. The electricity generated was analyzed and conversion efficiency was determined.

CHAPTER 2

LITERATURE REVIEW AND/OR THEORY

This section consists of four main segments which are overview of DSSC configuration, development of material as DSSC nanoparticles, the comparison between synthesis routes route and modification techniques to improve the properties of synthesis product.

2.1 OVERVIEW OF DEVICE CONFIGURATION (DSSC)

Dye-sensitized solar cells or DSSC belong to the group of thin-film solar cells. It is well-known as promising device to achieve moderate efficiency at ultra low-cost. DSSC consists of two major parts, which is photoelectron or photosensitive dye to absorb the light and semiconductor for charge transport. It is different from previous classical silicon thin-film cells where silicon act as photosensitive material and also for charge provider (Gratzel and Durrant, 1912). Refer to **Figure 1** for schematic diagram of DSSC's mechanism.

The basic element of a DSSC is a nanostructured material, an assembly of Titanium Dioxide nanoparticles that are well connected to their neighbors. TiO_2 is the preferred material since its surface is highly resistant to the continued electron transfer. However, TiO_2 only absorbs a small fraction of the solar photons (Bisquert et al. 2004). The mesoporous TiO_2 electrode is commonly a 10-mm-thick nanoparticulate film, with a three-dimensional (3D) network of interconnected 15–20-nm sized nanoparticles, leading to a huge surface area more than 1000 times larger than the projection surface. The large surface area of the nanoporous film enables efficient light harvesting, maximizing the amount of photogenerated charge (Li et al. 2009).

Molecular sensitizers or the dye molecules attached to the semiconductor surface are used to harvest a great portion of the solar light. The main dye molecules consist of one Ru metal atom and a large organic structure that provides the required properties like wide absorption range, fast electron injection and cell stability. The dye

is sensible to the visible light. The light creates the excitation in the dye that consists of highly energetic electron, which is rapidly injected to the TiO_2 particles (Bisquert et al. 2004).

Bisquert (2004) also mentioned that the nanoparticles semiconductor function as the transporter of light induced electrons towards the external contact, a transparent conductor that lies of the basis of the TiO_2 film. Because of the dye attached well to the whole TiO_2 surface, the nanostructure enhances the area that is used for collecting photons by a factor 100-1000, with respect to the device area.

Dye excitation is followed by electron injection into the TiO_2 and by dye re-charging via a redox electrolyte (mostly I^-/I_3^-). Electrons are transported in the TiO_2 nanoparticles to the front contact, which consists of a transparent conductive oxide layer (TCO). The contact to the redox electrolyte is made by a (catalyst-coated) back contact. For backside illumination,that contact can also be made transparent using a TCO window (Gratzel and Durrant, 1912).

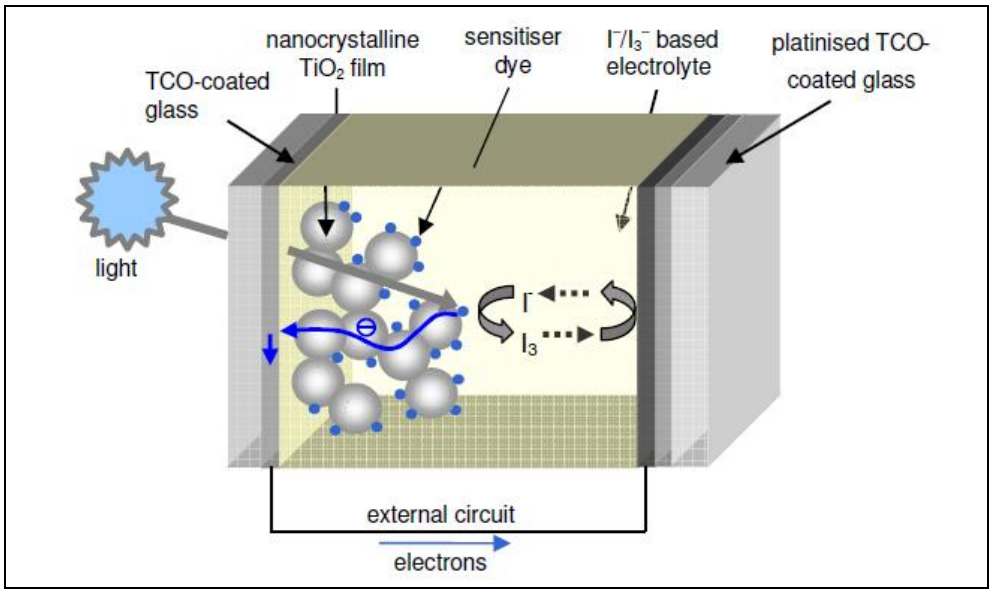

Figure 1: *Schematic diagram showing the mechanism of Dye Sensitized Solar Cell(Gratzel and Durrant, 1912.*

Figure 1 above shows the schematic diagram of a liquid electrolyte dye-sensitized solar cell. Gratzel and Durrant (1912) mentioned that the photoexcitation of

the sensitizer dye is followed by electron injection into the conduction band of the mesoporous oxide semiconductor, and electron transport through the metal oxide film to the TCO-coated glass working electrode. The dye molecule is regenerated by the redox system, which is itself regenerated at the platinised counter electrode by electrons passed through the external circuit.

A schematic diagram of the operating principles of the DSSC is given in **Fig. 1**. At the heart of the system is a mesoscopic oxide semiconductor film, which is placed in contact with a redox electrolyte organic hole conductor. The material of choice has been TiO_2 (anatase) although alternative wide band gap oxides such as ZnO, and Nb_2O_5 have also been investigated. Attached to the surface of the nanocrystalline film is a monolayer of the sensitizer. The latter result is the photo-excitation that results in the injection of an electron into the conduction band of the oxide. The dye is regenerated by electron donation from the electrolyte, usually an organic solvent containing a redox system, such as the iodide/triiodide couple. The regeneration of the sensitizer by iodide intercepts the recapture of the conduction band electron by the oxidized dye. The iodide is regenerated in turn by the reduction of triiodide at the counter-electrode the circuit being completed via electron migration through the external load. The voltage generated under illumination corresponds to the difference between the Fermi level of the electron in the solid and the redox potential of the electrolyte. Overall the device generates electric power from light without suffering permanent chemical transformation (Gratzel and Chimie, 2006).

In quantum efficiency terms, DSSC are extremely efficient. As mentioned by Okada et al. (2004), the depth of the nanostructure will increase the probability of the photon absorption and also the dye are very effective in converting the photon to electron. Most of the small losses exist in DSSC are due to conduction losses in the TiO_2 and the clear electrode, or optical losses in front of the electrode. The overall quantum efficiency is about 90% with the lost 10% largely accounted from optical losses in top electrode. The maximum voltage generated is simply the difference between Fermi level of the TiO_2 the redox potential of the electrolyte. Combined with a fill factor of about 45%, overall peak power production for current DSSC is about 11%.

Nanocrystalline titania exhibits photocatalytic activity in the presence of UV light, it can decompose organic pollutants and organic dyes such as methylene blue and rhodamine dye into CO_2, NH_4^+, NO_3^-, SO_4^{2-} and H_2O. The activity of titania will depend upon several factors, including electron–hole recombination, number of electrons created, phase composition (anatase or rutile), surface area, crystallinity and size of the TiO_2 and the absorption properties of the dyes on the surface of TiO_2 used. The silica doping will cause three main changes in the titania, which are anatase phase stability, increase in surface area and the band gap changes. Anatase titania has been reported to be more photocatalytically active than the rutile form because the adsorption affinity of organic dye molecule towards anatase phase is more compared to that towards rutile. The adsorption difference of the dye on TiO_2 is mainly due to the structural differences of anatase and rutile. As the specific surface area of the catalyst increases, it can adsorbed more dye molecules (Periyat et al. 2008).

2.2 DEVELOPMENT OF MATERIAL AS NANOPARTICLES

This section consists of the studies or researches that have done previously by other researchers on the development of Titanium Dioxide and the modification to improve the characteristic of nanoparticles. Several studies are included in this section, equipped with synthesize techniques, experimental procedures, experimental result and discussion. The synthesize techniques may include preparation of nanocrystalline by precipitation, reflux, sol-gel and hydrothermal. The focus here is to find the suitable synthesis method that can yield a stable product, with high absorption rate and high photocatalytic activity. Some modifications in the synthesis routes to improve the characteristic of final products are also included.

The first model of dye sensitized solar cell using titanium dioxide as the nanocrystalline. Titanium dioxide is widely known to have high photocatalytic activity, resistance to photocorrosion, photostability, low cost and non-toxicity (Lin et al., 2007).

It is usually prepared by hydrolysis of titanium compounds with subsequent thermal treatment or calcinations of the deposit formed (Voronsov, 2001). However, the available titanium oxides are poor absorbers of photons in the solar spectrum and only absorb the ultraviolet light, which constitutes only a small fraction (<5%) of the solar spectrum (Yin, 2001). The efficient utilization of solar energy is one of the major goals of modern science and engineering that will have a great impact on technological applications.

Significant progress and research has been done to improve the nanocrystalline of DSSC. Some of the method is by establishing junctions between titania and other semiconductors, doping with metals or ions and and composite design with porous materials and doping with non-metal compound. The modification on the synthesis parameter also influence the yield product. For example, the temperature of the treatment may influence the photocatalytic activity of TiO_2. The condition of measurement of TiO_2 photocatalytic activity can also give significant influence (Voronsov, 2001). For example, the photocatalytic activity of several compounds in liquid aqueous phase shown lower activity compared to the photooxidation in the gas phase. It was reported that the sparsely water soluble organics exhibit the highest oxidation rate over maximum calcinations temperature compared to highly water-soluble compounds that has very weak maximum calcinations temperature or just diminishes as the temperature rises (Tanaka et al. ,1993). This behavior attributed to the change in adsorption properties of TiO_2 with the growth of calcination temperature where the surface contains less OH groups and is capable to adsorb higher quantities of hydrophobic compounds and lower quantities of hydrophilic compounds.

The attempt to use the effect of calcinations temperature allows the control over the degree of crystal size, specific surface area and phase composition (Gorska et al., 2008).

Voronsov, et al. (2001) has done a study on the influence of TiO_2 calcination temperature on its bulk and surface structure in connection to the rate of deep oxidation of highly water-soluble compound, acetone, in the gas phase. The photocatalytic activity of TiO_2 samples prepared by aqueous hydrolysis of $TiCl_4$ and deposition with NH_3 in gaseous acetone photocatalytic oxidation has been found dependent on calcination temperature. The activity reaches its maximum at calcination temperature 450°C and then decreases when all the samples being anatase. The photocatalytic activity of the samples in a series of different calcination temperatures correlates well with reflectance of the samples in the visible light region. The increase in calcination temperature from 320 to 500°C results in the growth of TiO_2 crystallites, decrease in BET surface area, slight changes in lattice parameters, and removal of weak surface Bronsted acid centers. TiO_2 prepared by deposition with NaOH exhibits much higher photocatalytic activity. The observed correlation of diffuse reflectance and photocatalytic activity was attributed to opposite effects of the increase of crystallinity and removal of surface water and hydroxyl groups.

Various approaches to develop visible-light-activated TiO_2 have been investigated. Most attempts of TiO_2 modification have concentrated in doping a catalyst with selected additives. The earlier attempt of doping is between titania and transition metal. Surface recombination can be avoided by doping some foreign material like metal, non-metals and coupling titania with another semiconductor. Volume recombination can be reduced by preparing titania in nanoscale. Wavelength of maximum can also increased to higher wavelength by doping metals or non-metals (Vijayan, 2009). It is well known that wavelength and surface area are mainly depend on particle size. Altering the size of the particle alters the degree of confinement of the electrons, and affects the electronic structure of the solid, in particular ‘band edges’, which are tunable with particle size. However, the photocatalytic activity of metal doping is impaired by thermal instability (Choi et al., 1994) and an increase in carrier-recombination. Then, it has been found that doping with non-metal atoms, such as nitrogen, sulfur, fluorine, iodine and boron could successfully shift or extend TiO_2 absorption properties towards visible light (Asahi et

al., 2001). The catalysts were prepared by the sol–gel process using titanium alkoxide and ethanol with nitric acid as a catalyst, followed by calcination at certain temperature. Experimental results showed that about 70% of NO_x could be removed in the presence of a modified catalyst in a continuous flow type reaction system. A further study on titania doping lead to potential carbon doping synthesis technique (Hwang et al., 2006). A more substitutional carbon incorporation results in narrower band gap and hence better photocatalytic performance compared to a similar amount of nitrogen doping.

The research done by Wong et al. (2008) study the influence of crystallinity and carbon content on visible light photocatalysis of carbon doped titania thin films. Visible light responsive carbon doped TiO_2 films were developed by ion-assisted electron-beam evaporation using rutile powder as source material and two different gases, CO_2 and CO in the ion source as dopant source. This study demonstrates the effectiveness of using carbon monoxide (CO) and carbon dioxide (CO_2) gases for the preparation of carbon doped TiO_2 films by ion-assisted electron-beam evaporation. The beam current had a significant influence on the carbon content of the films and their crystallinity. At a beam current of 10 mA, the carbon doped TiO_2 film deposited using CO_2 gas is found to exhibit superior photocatalytic properties compared to other films. This is attributed to the optimum carbon incorporation with most favorable crystallinity in the film. An increase in titania crystallinity by annealing the films at 500 °C for 8 h gave favorable results in terms of photocatalytic performance. On the whole, the annealed carbon doped TiO_2 anatase film with the most doped carbon content of 1.25% gave the best visible light photocatalytic activity for superhydrophilicity, degradation of MB and reduction of silver ions.

The study done by Shao et al. (2008) was to fabricate the spontaneously hierarchically formed mesoporous-macroporous N-doped titania material by thermal treatment of with urea solution, in order to extend their photocatalytic application from ultraviolet to visible-light range. In this work, nitrogen-doped titania with hierarchical meso-macroporous structure was prepared as active visible-light photocatalyst by nitridation of template-free synthesized mesomacroporous titania using urea as a

nitrogen donor. The resultant meso-macroporous $TiO_{2-x}N_x$ exhibited a bicrystalline (anatase and brookite) framework with high surface area and large porosity. The enhancement of photocatalytic activity of meso-macroporous titania was observed due to the increasing photoabsorption efficiency and efficient diffusion of molecules caused by the macropores.

The titania samples, prepared by the hydrolysis of tetrabutyltitanate in the absence of surfactant and autoclaving at 60–80 ^{o}C, are mainly tens to several tens of micrometers in size with irregular shapes, but with a macroporous structure. The macro channels are arranged parallel to each other and perpendicular to the tangent of the surface of the particles, with the length of 2–8 mm; and the macroporous framework is composed by the assembly of small particles, leaving small holes in the macropore-walls of 300–800 nm in thickness.

When the autoclaving temperature increased to 80 ^{o}C, an alternatively macroporous structure with smaller macropore size of 125–250 nm was obtained. This indicates that the elevated autoclaving temperature resulted in different microphase separation process for the spontaneous formation of macroporous structure. FT-IR and XPS spectra are collected to study the surface chemistry of the photocatalysts. The results indicated that the treatment of the MMTD precursor with urea resulted in not only the chemisorption of NH3 molecules on the TiO2 surface but also the nitridation of the TiO2 in network. The MMTD showed a good photocatalytic activity in the degradation of dye molecules, while the photocatalytic activities of nitrogen-doped samples were significantly improved with an increase of the actual nitrogen doping concentration. The efficiency of the photocatalytic degradation of MO under UV irradiation, as well as in the photodegradation of RhB under visible-light irradiation on the N-T-x/y samples is much better than that of the MMTD.

The enhancement of the photocatalytic activity of nanosized TiO_2 materials has been pursued by doping with transition metals to modify the band-gap energy (Zorn et al, 2001), or by establishing junctions between different phases (metal–semiconductor or semiconductor–semiconductor) in order to reduce charge recombination (Kawahara

et al., 2002). In particular, considerable improvement of the photocatalytic activity of TiO_2 has been achieved by incorporating other semiconductors with larger band gap width like SnO_2 or ZrO_2 (Zorn et al., 2001). In this respect, sol–gel-derived TiO_2–ZrO_2 thin films present high activities for the photocatalytic oxidation of ethylene and acetone vapor. Similarly, TiO_2–ZrO_2 photocatalysts prepared as powders are more efficient than pure titania for the removal of organic pollutants in either aqueous solutions or in the gas phase (Shchukin, 2003). The increase in surface area with respect to TiO_2 at a given firing temperature, the inhibition of rutile formation, the rise in surface acidity or the creation of active defects on the TiO_2 surface have been proposed as possible causes of this improvement.

Quan Yuan et al. (2009) have done a study on the synthesis of highly ordered mesoporous titania–zirconia composites with broad Ti/Zr ratios via an evaporation-induced self assembly (EISA) process. The whole process is self-adjusting to organize the network-forming metal oxide species without extra acid or base. The highly ordered mesoporous structures with 2D hexagonal symmetry are obtained by adjusting the amounts of structure directing agents (SDAs) under a proper relative humidity and evaporation temperature. A series of titania–zirconia nanocomposites with controlled texture properties and composition are obtained in a wide range from 10 to 90 mol% TiO_2 through tuning the initial mass ratios. The composites possess ordered 2D hexagonal mesostructure, high surface area (up to 200 $m^2\ g^{-1}$), large pore volume (0.1–0.3 $cm^3\ g^{-1}$), and uniform pore size (3.5–4.1 nm). The titania-zirconia composites show good photocatalytic activities for photodegradation of rhodamine B and hydrogen evolution in an aqueous suspension, which can be acknowledged to the cooperative effect of the crystallinity and porosity of these materials.

Hidalgo et al. (2007) did a study on photocatalytic properties of un-doped and iron-doped ZrO_2-TiO_2 catalysts. The local zirconium and iron arrangements of the iron-doped ZrO_2-TiO_2 system, prepared by sol–gel impregnation method, were studied by EXAFS spectroscopy. This study represents an example of attempt to prepare a new

potential photoactive mixed oxide system, containing two ions (Ti^{4+} and Zr^{4+}) with good photocatalytic activity if it is compared with commercial TiO_2 calcined at 600 °C.

For the iron-doped ZrO_2-TiO_2 system, the presence of the Fe-O-Fe species as well as Fe-O-Zr species located on the surface/pre-surface region shown that iron is heterogeneously distributed, forming small iron oxide nanoclusters and Fe_x/ZrO_2 (tetragonal) spots at the catalyst surface. However, it is clear that incorporation of Fe^{3+} species on the binary system ZrO_2-TiO_2 results unfavorable for the photocatalytic activity in both cases, salicylic acid photooxidation and photoreduction of Cr(VI). The preparation and photocatalytic properties of Zr^{4+}-doped TiO_2 nanocrystals have been recently reported . It was shown that when the Zr^{4+} content was 6 mol%, the photocatalytic efficiency of $Ti_{0.94}Zr_{0.06}O_2$ was 1.5 times higher than that of pure TiO_2. However, for this kind of system, prepared by sol–gel method, the doping species Zr^{4+} was incorporated into the TiO_2 lattice leading to larger lattice deformation and forming capture traps, which contribute to the higher separation efficiency of the photogenerated carriers.

The photocatalytic properties of a prepared zirconium titanate, $ZrTiO_4$, was investigated and comparison with the parent oxides TiO_2 and ZrO_2 was reported. In that case, the following activity order, independently of the substrate considered, was found: $TiO_2 \gg ZrO_2 > ZrTiO_4$. Thus, titania, especially in the anatase form, is the most active solid. The least active solid is $ZrTiO_4$. Since, ZrO_2 absorbs at much shorter wavelengths, it can be proposed that, for a given flux, the smaller amount of photons absorbed by ZrO_2 can generate more efficient electron–hole pairs, which preferentially separate instead of recombining. At the same time, ZrO_2 possesses good adsorptive properties with respect to the reactants, thus favouring reactions on the adsorbed phase and compensating for its lower absorbance in the UV range. It seems to be clear that the core-shell ZrO_2-TiO_2 binary system is a good alternative for TiO_2 and consequently for $ZrTiO_4$.

The study done by Maria et al. (2006) focused to study the influence of phase composition to the photocatalytic activity. Acidic solutions of different composition

(ZrO_2, TiO_2 and Ti–Zr mixed oxides) have been prepared using metal alkoxides as starting materials. The photoactive oxides were deposited on "Raschig rings" of borosilicate glass using a dip-coating technique. The phase composition of the thin films was controlled during the solution preparation stage to produce either (1) $Ti_{0.90}Zr_{0.10}O_2$ solid solutions, or (2) ZrO_2/TiO_2 binary metal oxides (10% and 20% molar content of Zr). As usual, the characterization technique was applied using the Raman spectroscopy, TGA-DTA, and UV vis-spectra. The results obtained in the present study indicate that sol–gel synthesis is an adequate method of preparing nanocrystalline TiO_2–ZrO_2 thin-films with controlled structure and porosity. In all cases, the incorporation of Zr leads to notable increase in surface area with respect to TiO_2, and it also contributes to stabilising the anatase phase. The photocatalytic oxidation of acetone in dry air over the glass rings coated with TiO_2–ZrO_2 thin films was studied using a recirculating photo-reactor. In contrast, a further increase of the ZrO_2 content is unfavorable to the photocatalytic performance of the thin films, as indicated by the lower rate obtained over the ZrO_2/TiO_2 (20% Zr) rings. A second series of measurements of photocatalytic activity was performed in a continuous flow reactor using a humid oxygen stream containing methylcyclohexane (MCH) as a model pollutant. In this case, no conversion of MCH was detected under UV-illumination in absence of photocatalyst. The higher photocatalytic oxidation rate corresponds to the ZrO_2/TiO_2 (10% Zr) sample. In contrast, the photoactivity for eliminating MCH is higher for the sample M2 than for M1, despite its higher surface area. It can be summarize that the increment of surface area does not correlate with a photoactivity rise. The slightly higher photoactivity of ZrO_2/TiO_2 (10% Zr) thin films suggests that the formation of separate ZrO_2 and TiO_2 phases can be beneficial for these processes. The changes in the texture or the density and nature of the surface groups (e.g. acidity) can have a significant influence on the photoactivity of these thin films. Crystallization of $ZrTiO_4$ and formation of rutile appears to be almost simultaneous process. The excess of titanium give rise apparently to the solid solution into $ZrTiO_4$ and transition to crystalline $ZrTiO_4$ as shifts to higher temperature. Further increase of heating treatment temperature leads to narrower and

intense diffraction that indicate further growth and size increase of anatase nanocrystals and resulting in the collapse of the mesostructure.

Table 1: *XRD data from the study done by Daturi et al.*

Sample	*T calc. (K)*	*XRD phase*	*Cell parameters (Å)*			
			a	*b*	*c*	β
ZrO_2	623	Amorphous	—	—	—	—
	723	Tetragonal	5·112 (7)	—	5·200 (15)	—
		Monoclinic	5·298 (8)	5·219 (11)	5·153 (4)	98·71 (0·06)
	1273	Monoclinic	5·317 (4)	5·213 (3)	5·158 (3)	99·19 (0·02)
		Tetragonal	5·126 (10)	—	5·306 (9)	—
$Zr_{0.95}Ti_{0.05}$	393	Amorphous	—	—	—	—
	723	Tetragonal	5·097 (2)	—	5·174 (9)	—
		Monoclinic	5·313 (9)	5·248 (7)	5·152 (5)	99·16 (0·05)
	1273	Monoclinic	5·297 (5)	5·220 (4)	5·145 (4)	99·23 (0·02)
		Tetragonal	5·082 (9)	—	5·298 (12)	—
$zR_{0.90}Ti_{0.10}$	393	Amorphous	—	—	—	—
	723	Tetragonal	5·074 (2)	—	5·191 (5)	—
		Monoclinic	5·320 (10)	5·220 (7)	5·135 (6)	99·09 (0·05)
	1273	Monoclinic	5·278 (8)	5·206 (6)	5·097 (7)	99·03 (0·05)
		Tetragonal	5·052 (14)	—	5·257 (12)	—
$Zr_{0.75}Ti_{0.25}$	393	Amorphous	—	—	—	—
	723	Tetragonal	5·105 (6)	—	5·142 (17)	—
		Monoclinic	5·291 (4)	5·177 (6)	5·178 (14)	98·57 (0·07)
	1273	Tetragonal	5·057 (1)	—	5·218 (3)	—
		Monoclinic	5·294 (6)	5·213 (4)	5·125 (4)	98·77 (0·03)
$Zr_{0.50}Ti_{0.50}$	393	Amorphous	—	—	—	—
	723	Amorphous	—	—	—	—
	1273	$ZrTiO_4$	5·021 (5)	5·454 (4)	4·844 (5)	—
$Zr_{0.25}Ti_{0.75}$	393	Anatase	3·800 (3)	—	9·554 (11)	—
	723	Anatase	3·806 (3)	—	9·621 (17)	—
	1273	Rutile	4·619 (1)	—	2·986 (3)	—
		$ZrTiO_4$	5·008 (5)	5·491 (6)	4·774 (8)	
$Zr_{0.10}Ti_{0.90}$	393	Anatase	3·790 (2)	—	9·466 (9)	—
	723	Anatase	3·803 (3)	—	9·569 (15)	—
		Brookite traces	—	—	—	—
	1273	Rutile	4·623 (1)	—	2·987 (1)	—
		$ZrTiO_4$ traces	—	—	—	—
$Zr_{0.05}Ti_{0.95}$	393	Anatase	3·781 (2)	—	9·427 (8)	—
	723	Anatase	3·776 (3)	—	9·526 (12)	—
		Brookite traces	—	—	—	—
	1273	Rutile	4·591 (2)	—	2·968 (2)	—
		$ZrTiO_4$ traces	—	—	—	—
TiO_2	393	Anatase	3·781 (4)	—	9·413 (11)	—
	723	Anatase	3·784 (2)	—	9·454 (6)	—
		Brookite traces	—	—	—	—
	1273	Rutile	4·592 (2)		2·959 (0)	

Table 1 shows the XRD data obtained from the study done by Daturi. Daturi et al. have characterized the $ZrTiO_4$ powders by coprecipitation method, and the result has shown that the addition of titania to the pure zirconia precipitate modifies progressively

the crystallization behavior of zirconia. Meaning that titania favours the formation of monoclinic versus tetragonal zirconia, although the main effect is the inhibition of the crystallization of either ZrO_2 phases. The sample with equimolar amount of TiO_2 and ZrO_2 looks completely amorphous until near 970K when $ZrTiO_4$ appears by a fast crystallization process. It is also shown that ZrO_2 clearly interferes with the transformation of anatase into rutile, the thermodynamic stable titania polymorph.

Based on the synthesis method above, it can be summarized that almost all synthesis method successful in producing zirconium titanate with unique physical and chemical characteristic. The selection of the best synthesis route should depending on several information: the initial material used, the period of time required to produce the product, the complication of the process route (eg: calcinations temperature, equipment required) and the most important is the characteristic of yield product (eg: photocatalytic activity, stability). However, several modifications could be applied to enhance the result of yield product. The modification will be elaborated in the subdivision 2.4 below.

2.3 COMPARISON BETWEEN SYNTHESIS ROUTES

The common synthesis route of producing Zirconium Titanate is by hydrothermal, sol-gel process, hydrolysis and precipitation. This section discussed on the advantages and disadvantages of each synthesis routes. The hydrolysis route is not included since it was almost usually incorporated with sol-gel process. In addition, the alternative process route which is combination between hydrothermal and sol-gel is explained in the **Table 2** below.

Table 2: *Summary of comparison between synthesis routes.*

Synthesis route	Remarks
Hydrothermal	• The hydrothermal process including aqueous solvents as reaction medium is eco-friendly since it is carried out in a closed system and the contents can be recovered and reused after cooling down to room temperature. • The equipment and processing required are simpler and reaction is low energy consumption, • By controlling hydrothermal temperature and duration of the treatment, various crystalline products with different composition, structure and morphology could be obtained. • Fine particle size can be obtained with more uniform distribution and high dispersion either in polar and nonpolar solvents • In this way the energy band structure becomes discrete and titania nanoparticles exhibit improved optical and photocatalytic properties. • Have more uniform distribution in particle size. High purity and reduced particle size is not possible in hydrothermal methods.
Sol-gel	• Generation of a dispersion of colloidal particles suspended in Brownian motion within a fluid matrix. • Colloids are suspension of particles of linear dimensions between 1nm and 1 μm. The colloidal suspensions can subsequently convert to viscous gels and then to solid materials • Sol-gel preparation leads to the greatest possible homogeneous distribution of the dopant ion in the host matrix. • Products have high purity and homogeneity, ease of processing and composition control and cost effective • Process steps: Ageing, Gelation, Drying, Densification

	• Sol-gel method can be used for the preparation of nanosized titania with high purity but size restriction is not possible anywhere in the preparation procedure. Sol-gel method does not produce phase purity.
Sol-gel followed by hydrothermal	• Materials can be obtained with high purity • Particle size can be reduced and controlled • Highly crystalline material can be obtained • Material with higher light harvesting character • Phase formation can be decided before the heat treatment i.e, calcination • Eco-friendly
Precipitation	• Easy and cost effective • Preparation of very small particles and ability to control the particle size. • The disadvantage is low production yield and need to use large amount of solvents and surfactants.

It can be summarized that the synthesis process that involved heat treatment lead to better yield of product.

2.4 Modification techniques that can be applied to improve the characteristic of $ZrTiO_4$

The research done by Kobasa and Kondrat'eva (2006) mentioned that there were relationship found between photocatalytic activity (PCA), absorption spectra, electrical conductivity (σ), and catalytic activity (CA) for oxides containing Zr^{4+} and Ti^{4+} and their quantitative and phase composition. It was found that PCA and CA depend

linearly on the σ. The utilization of the relation will help to improve the result for characteristic of zirconium titanate as the nanocrystalline in DSSC.

The focus in this study is to improve the absorption spectra and improve photocatalytic activity of zirconium titanate as the DSSC nanocrystalline, thus increasing the effectiveness of DSSC. Based on the development of the synthesis routes of $ZrTiO_4$ included in the section above, it can be summarized that the characteristic of $ZrTiO_4$, or specifically the photocatalytic activity is affected by several parameters. The parameters includes the initial composition of the copolymers and metal precursors, the calcinations temperature used during synthesis, and the additive used in the synthesis.

Table 3: *Summary of modification and parameter that has significant effect to characteristic of nanocrystalline.*

Parameter/Modification	Effect
Calcination temperature (Voronsov, 2001)	Increasing calcinations temperature will increase PCA until a maximum point (estimated 600^{o}C and above)
Crystallinity & carbon content (Wong, 2008)	Using CO and CO_2 gases for the preparation of carbon doped TiO_2 films by ion-assisted electron-beam evaporation. The increase of both crystallinity & carbon content shown significant increase in PCA. (eg: annealing at temp 500^{o}C in 8 hours and carbon doped content of 1.25%).
Adjustment of initial molar ratio of copolymers to metal precursors (Quan Yuan, 2009)	Yield nanocomposites with controlled texture and composition. The porosity and crystallinity of nanocrystalline give significant effect to PCA.
Additive or doping material example: Ferum (Hidalgo, 2007) & Phosphorus (Lin, 2007)	The selection of additive is crucial. For example addition of Ferum is unfavorable since it reduces the PCA. But, the addition of Phosphorous increase the surface area of material, thus increase the content of hydroxyl group. It also improved thermal

	stability and decrease phase transformation from anatase to rutile. More importantly, the nanocrystalline is active under visible light, most possibly due to high surface area and small crystallinity size.
Nitrogen donor example: Urea (Shao, 2007)	Use urea as nitrogen donor. Yield nanocrystalline with high surface area and large porosity, that leads to higher photoabsorption & diffusion efficiency, thus increase PCA in visible light.
Influence of phase composition (Maria, 2006)	Change in texture, density, surface group (eg:acidity) give significant effect to PCA. The study suggests that the formation of separate ZrO_2 and TiO_2 phases can be beneficial to PCA.

CHAPTER 3

METHODOLGY/PROJECT WORK

This chapter described the experimental techniques, apparatus used, as well as the analytical methods undertaken in the course of this study to achieve the objective mentioned previously. The proposed experimental procedure to synthesize Zr/TiO_2 nanoparticles is included in this chapter. The included experimental procedures are based on the previous study and research done by other researchers. At the end of this chapter, the characterization techniques for the product of synthesis was discussed.

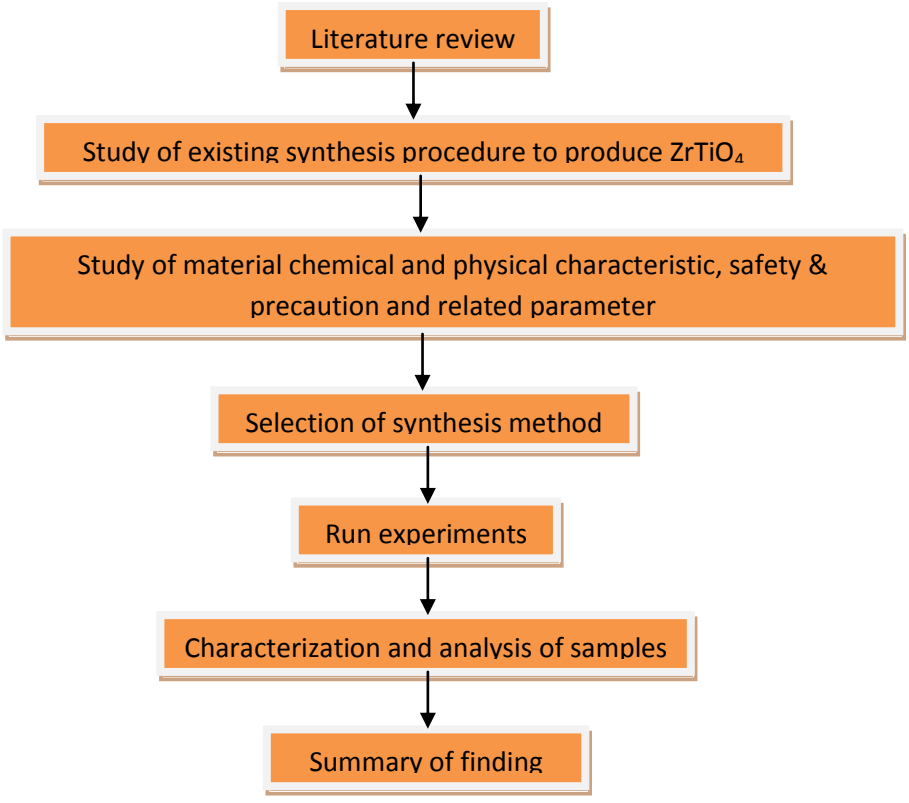

Figure 2: *Work flow for research.*

3.1 PROCEDURES OF SYNTHESIS ROUTES

Based on the study on literatures, two synthesis methods was found to be suitable and selected for the study. The synthesis procedures included in this section are procedures for impregnation and reflux method.

3.1.1 Preparation of $ZrTiO_4$ by Reflux method

The first set of sample of specified molar concentration of Zirconyl Nitrate and Titanium (IV) Oxide are used to prepare each ZT samples. The metal salts are dissolved with 100mL deionized water, stirred for 30 minutes and was refluxed at 100^{o}C for 4 hours. Then mixture will be dried in oven at 120^{o}C overnight and later calcined at 600^{o}C for 6 hours. Several set of samples were produced by using different molar ratios (**see Table 4**).

Table 4: *Data for reflux sampling.*

Sample	Molar ratio (mol Zr/mol Ti)	Mass ratio (g Zr/g Ti)
1	1.00 : 1.00	57.81 : 20.00
2	1.00 : 0.5	57.81 : 10.00
3	0.5 : 1.00	28.91 : 20.00

Figure 4: *Raw material used for the experiment (Zirconyl nitrate & Titanium (IV) oxide)*

Figure 3: *Mixture of chemicals stirred using stirring hotplate for 30 minutes.*

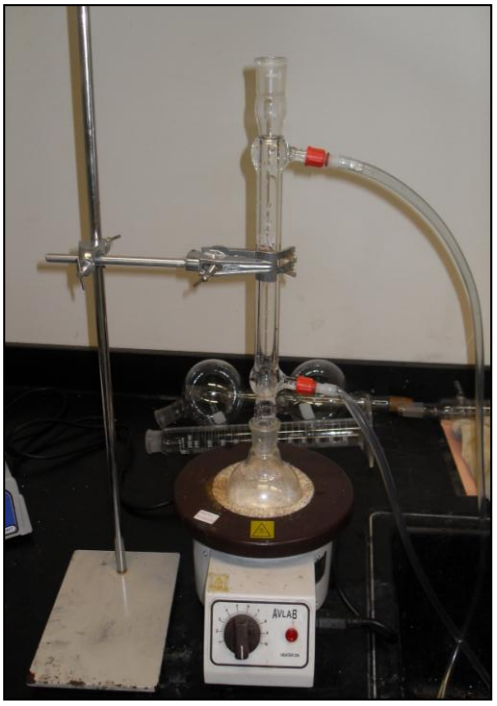

Figure 5: *The fluid mixture was refluxed at 100^{o}C for 5 hours.*

3.1.2 Preparation of $ZrTiO_4$ by Impregnation method

The first set of specified molar concentration of zirconyl nitrate and titanium oxide are used to prepare each ZT samples. The metal salts are dissolved with 100 mL deionized water and was stirred for 4 hours by using magnetic stirrer. Then the mixture will be dried in oven 120^{o}C overnight and later calcined at 600^{o}C for 6 hours. Several set of samples were produced by using different molar ratios (**see Table 5**).

Table 5: *Data for impregnation sampling.*

Sample	Molar ratio (mol Zr/mol Ti)	Mass ratio (g Zr/g Ti)
4	1:1	57.81/20.00
5	1.00 : 0.5	57.81 : 10.00
6	0.5 : 1.00	28.91 : 20.00

Figure 7: *The chemical mixture was stirred for 5 hours in room temperature.*

Figure 6: The product yield was dried in the oven for overnight at temperature of 120^{o}C.

Figure 3.7: *The dried product was calcined in furnace at temperature 600^{o}C for 6 hours.*

Table 6: *Summary of samples used in the study***.**

Reff No	Sample Name	Synthesis Method	Composition Raw Material	Calcination
1	MI CI C	Reflux	1:1	YES
2	MI SII C	Reflux	1:0.5	YES
3	MI SIII C	Reflux	0.5:1	YES
4	MI CI XC	Reflux	1:1	NO
5	MI SII XC	Reflux	1:0.5	NO
6	MI SIII XC	Reflux	0.5:1	NO
7	MII SI C	Impregnation	1:1	YES
8	MII SII C	Impregnation	1:0.5	YES
9	MII SIII C	Impregnation	0.5:1	YES
10	MII SI XC	Impregnation	1:1	NO
11	MII SII XC	Impregnation	1:0.5	NO
12	MII SIII XC	Impregnation	0.5:1	NO

The summary of sampling preparation is listed at **Table 6**.

3.2 CHARACTERIZATION TECHNIQUES

The characterization analysis will be done to analyze the product of synthesis, $ZrTiO_4$ after the synthesis of product completed. Several parameters have been determined and will be analyze using specified characterization techniques. Below are the characterization techniques that will be use in this study:

3.2.1 X-ray diffraction (XRD)

X-ray scattering techniques are a family of non-destructive analytical techniques which reveal information about the crystallographic structure, chemical composition, and physical properties of materials and thin films. These techniques are based on observing the scattered intensity of an X-ray beam hitting a sample as a function of incident and scattered angle, polarization, and wavelength or energy. X-ray diffraction finds the geometry or shape of a molecule using X-rays. X-ray diffraction techniques are based on the elastic scattering of X-rays from structures that have long range order. The most comprehensive description of scattering from crystals is given by the dynamical theory of diffraction.

X-ray powder diffraction patterns of 8 samples treated at temperature 600^oC were recorded in the region of 2θ = 10-80^o with a screening speed of ¼ ^{o} min^{-1} on a Philips diffractrometer (Model PW 1710) using CuK_α radiation with a nickel filter. The average size of the crystallite in sample is calculated using the Scherrer equation.

$$\textbf{Average particle size, } D = k\lambda/h_{1/2}\cos\theta$$

Figure 8 shows the XRD study done by Baochao (2008). Based on the study, it was observed that several stronger diffraction peaks at 25^{o} assigned to the anatase phase of TiO_2 and small diffraction at 30^{o} corresponding to ZrO_2 tetragonal phase.

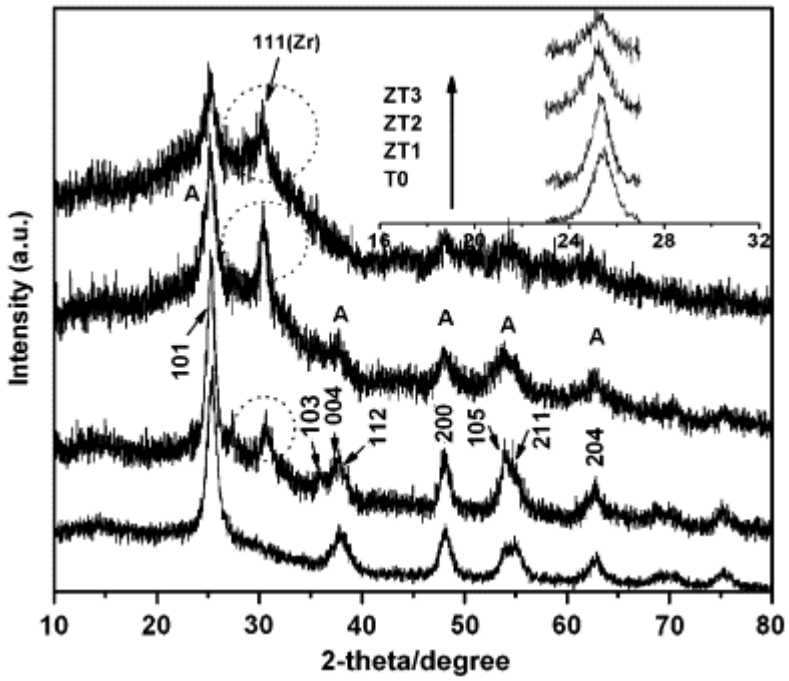

Figure 8: *The product yield was dried in the oven for overnight at temperature of 120^{o}C.*

The XRD result obtained this study was compared to the study done by Baochao.

3.2.2 Raman spectroscopy

Raman Spectroscopy is a spectroscopic technique used to study vibrational, rotational, and other low-frequency modes in a system. It relies on inelastic scattering, or Raman scattering, of monochromatic light, usually from a laser in the visible, near infrared, or near ultraviolet range. The laser light interacts with phonons or other excitations in the system, resulting in the energy of the laser photons being shifted up or down. The shift in energy gives information about the phonon modes in the system.

3.2.3 Scanning electron microscope (SEM)

SEM is a type of electron microscope that images the sample surface by scanning it with a high-energy beam of electrons in a raster scan pattern. The electrons interact with the atoms that make up the sample producing signals that contain information about the sample's surface topography, composition and other properties such as electrical conductivity. The types of signals produced by an SEM include secondary electrons, back-scattered electrons (BSE), characteristic X-rays, light (cathodoluminescence), specimen current and transmitted electrons.

Morphology and elemental analysis of the samples were carried out on Cambridge Stereoscan (Model 999) equipped with an energy dispersive X-Ray analyser. Conducting samples were prepared by either coating carbon or sputtering gold on finely ground powder specimen. The magnification set for visual view was 20K, WD set to 5mm and EHT 15kV. Samples selected for visual analysis was sample 1 to sample 7.

3.2.4 Diffuse Reflectance UV-Visible (DRUV)

The DRUV spectrophotometer, is a valuable tool used to characterize a variety of materials. The accessory provides sample mounting configurations for performing both reflectance and transmission measurements. With this accessory, we easily measure a myriad of materials from solids to liquids. The sample size is nearly unlimited, greater than 99% reflectance from 400 nm to 900 nm and greater than 95% reflectance from 250 nm to 900 nm.

Figure 9 below shows the DRUV-vis study done by Mishra et al. (2008). It is observed that with the mixture of zirconia and titania, the absorption band is extended to the visible range. The TiO_2 only absorbs UV light.

Note: 1) Visible light range : 400-720 nm (Cesare,1987)

2) UV light range : 10-400 nm

It is expected that with addition of Zirconia to the Titanium Dioxide, the absorption band will be extended to the visible range.

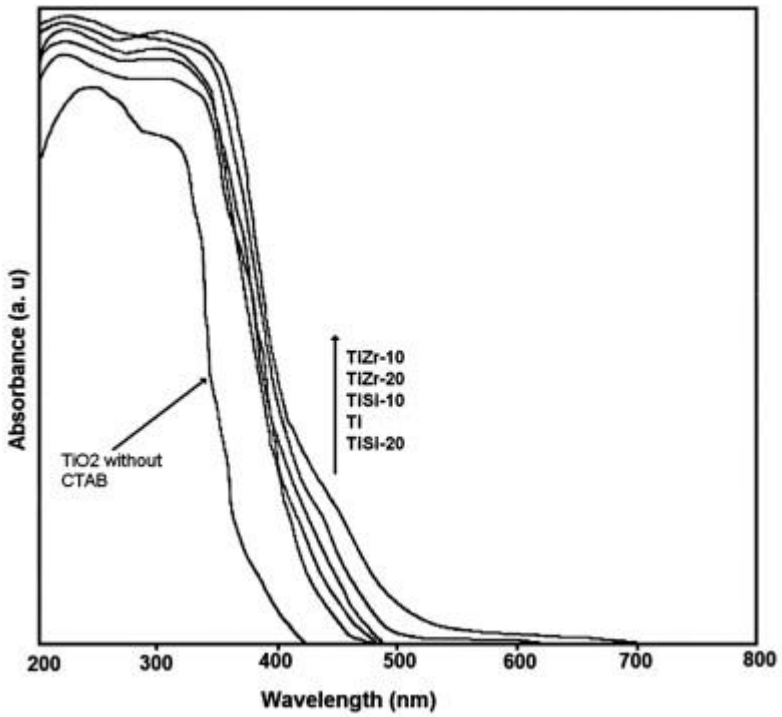

Figure 9: *DRUV-vis study done by Mishra (2008).*

3.2.5 Fourier Transform InfraRed (FTIR)

In infrared spectroscopy, IR radiation is passed through a sample. Some of the infrared radiation is absorbed by the sample and some of it is passed through (transmitted). The resulting spectrum represents the molecular absorption and transmission, creating a molecular fingerprint of the sample. Like a fingerprint no two unique molecular structures produce the same infrared spectrum. This makes infrared spectroscopy useful for several types of analysis. First, it can identify unknown materials. Second, it can determine the quality or consistency of a sample. Third, it can determine the amount of components in a mixture.

The interpretation of FTIR result are based on the Table A at **Appendix A**.

3.2.6 Brunauer, Emmett and Teller,BET

BET (Brunauer-Emmet-Teller) method is based on adsorption of gaseous molecules on particles surface. The powder is evacuating and heating to about 200ºC, after that nitrogen or xenon is adsorbing in liquid nitrogen temperature. Surface of sample is calculating by Brunauer-Emmet-Teller equation. The application of BET is to deteremine the pore size distribution analysis, average pore volume, area, size and Total Pore Volume (TPV) powders of inorganic materials, oxides, sorbents, catalysators.

3.2.7 X-Ray Photoelectron Spectroscopy (XPS)

XPS is a surface chemical analysis technique that can be used to analyze the surface chemistry of a material. XPS can be used to measure elemental composition of the surface, empirical formula of pure materials, elements that contaminate a surface, chemical or electronic state of each element in the surface, uniformity of elemental composition across the top surface and uniformity of elemental composition as a function of ion beam etching.

3.2.8 Application on Test Cell

At the end of characterization, a test cell will be developed using the synthesized nanoparticles and a study on the electricity generated will be performed.

CHAPTER 4

RESULTS AND DISCUSSIONS

This chapter discusses the experimental result and analysis of the finding. The effects of process parameters such as calcinations temperature and synthesis method are explained.

4.1 EXPERIMENTAL RESULTS

The sampling procedure, which involved two synthesis methods (reflux and impregnation) was completed. **Figure 11** and 1**2** below shows the product from both reflux and impregnation method before and after calcinations.

Figure 11:*The product yield after dried in the oven for overnight at temperature of 120^{o}C***.**

Figure 10: *The product yield after calcinations at temperature 600^{o}C for 6 hours.*

After calcinations, it is estimated that the nitrate compound and hydroxyl group will be eliminated from the samples. The assumption will be proven by XRD analysis and FTIR.

4.1.1 SEM Results

SEM images shows homogenously porous material in ceramics sintered at 600 °C. It can be seen that by the variation of Zirconia/Titania ratio changes the microstructure and the fracture behaviour. Larger fractured surface and smaller pores can be seen in the Sample MI SIII C and Sample MII SIII C. It is parallel to the study done by Ussui et al. They mentioned that with the higher concentration of Zirconia, the smaller are the grain size and more uniform is fractured surface. Opposite to sample with higher concentration of titanium, they yield worse ceramic sinterability. By comparing to the Sample MI SI XC which was not calcined, it showed that by calcinations, it lead to progressive reduction of porosity and grain size. Based on Gajovic et al. lower porosity and larger sintered grains were obtained at higher sintering temperatures. In material sintered at higher calcinations temperature the sintered grains continue to enlarge and become welded making a continuous ceramic structure, and thus causing the ability for closing the pores inside the material.

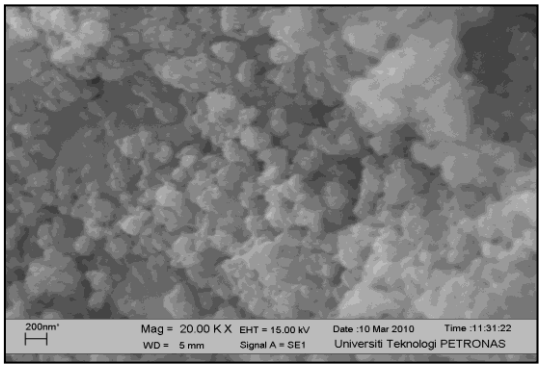

(a)

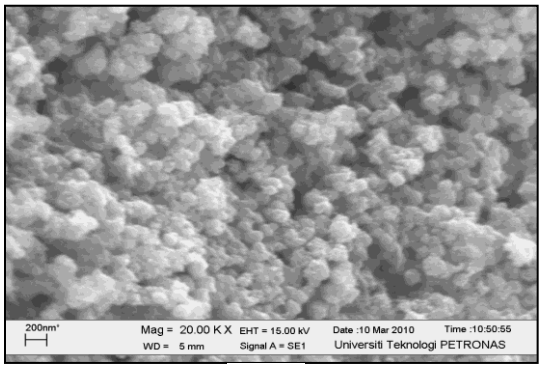

(b)

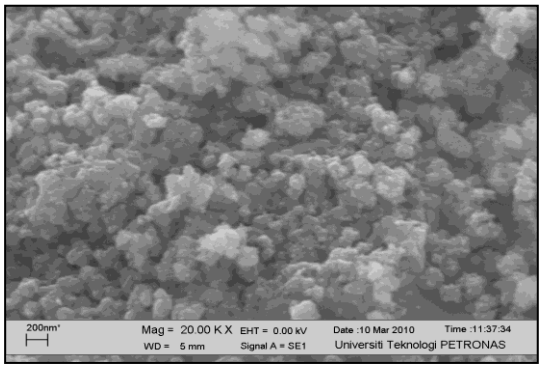

(c)

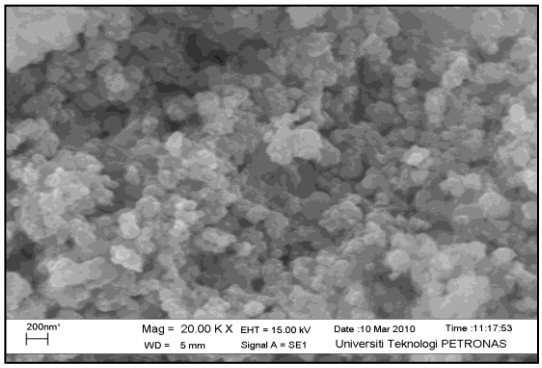

(d)

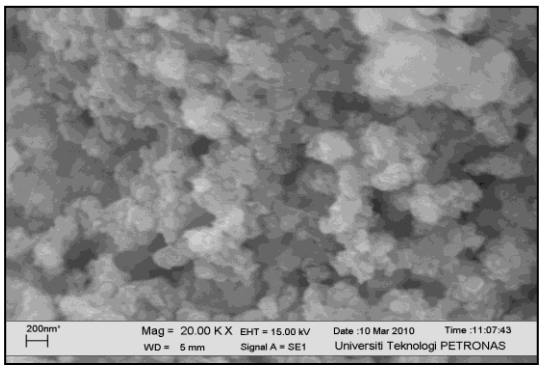

(e)

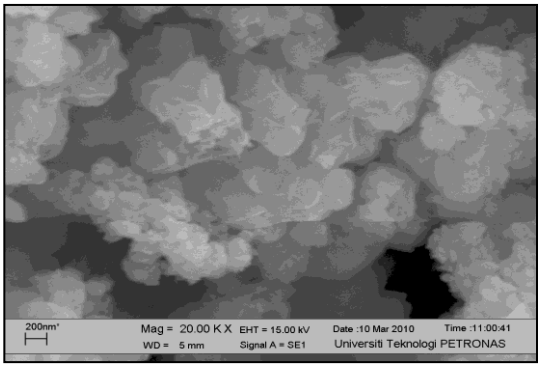

(f)

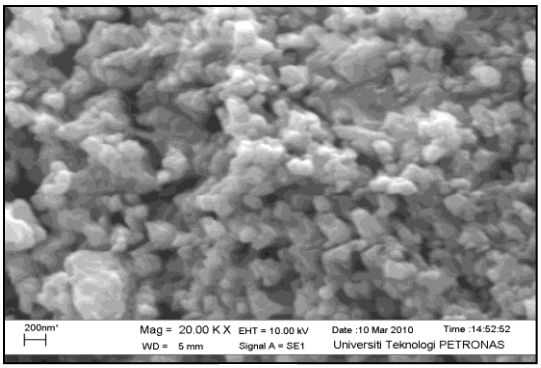

(g)

Figure 12: *SEM micrographs of ceramic surface of samples a) MI SI C; b) MI SII C; c) MI SIII C; d) MII SI C; e) MII SII C; f) MII SIII C; g) MI SI XC*

Figure 12 above shows the image from SEM analysis at 20K magnification.

4.1.2 Raman Spectroscopy Results

Figure 13 below shows the plot of Raman spectra of $ZrTiO_4$ that has been calcined at temperature 600^oC in 6 hours. For clearer information regarding the plot, refer to **Table 7** below.

$ZrTiO_4$ with orthorhombic symmetry (space group *Pbcn*) and two formula units in a unit cell has 33 optically active modes of vibration, 18 of which are Raman active (J. Macan). Only $ZrTiO_4$ bands were observed in 20–800 cm^{-1} region of the Raman spectra. The bands for all the samples are broad, which can be attributed to random distribution of Zr^{4+} and Ti^{4+} ions in equivalent sites of crystal lattice, oxide defects and nonstoichiometric variations of Zr/Ti ratio in polycrystalline ceramics (F. Azough). It is observed that the peak intensity and width of plot vary with the content of the samples. The character shown by sample MI SII C, which has the highest intensity and broad distribution indicate higher ordering due to small possible amount of low temperature $ZrTiO_4$ phase of high structural order (Gajovic et al.).

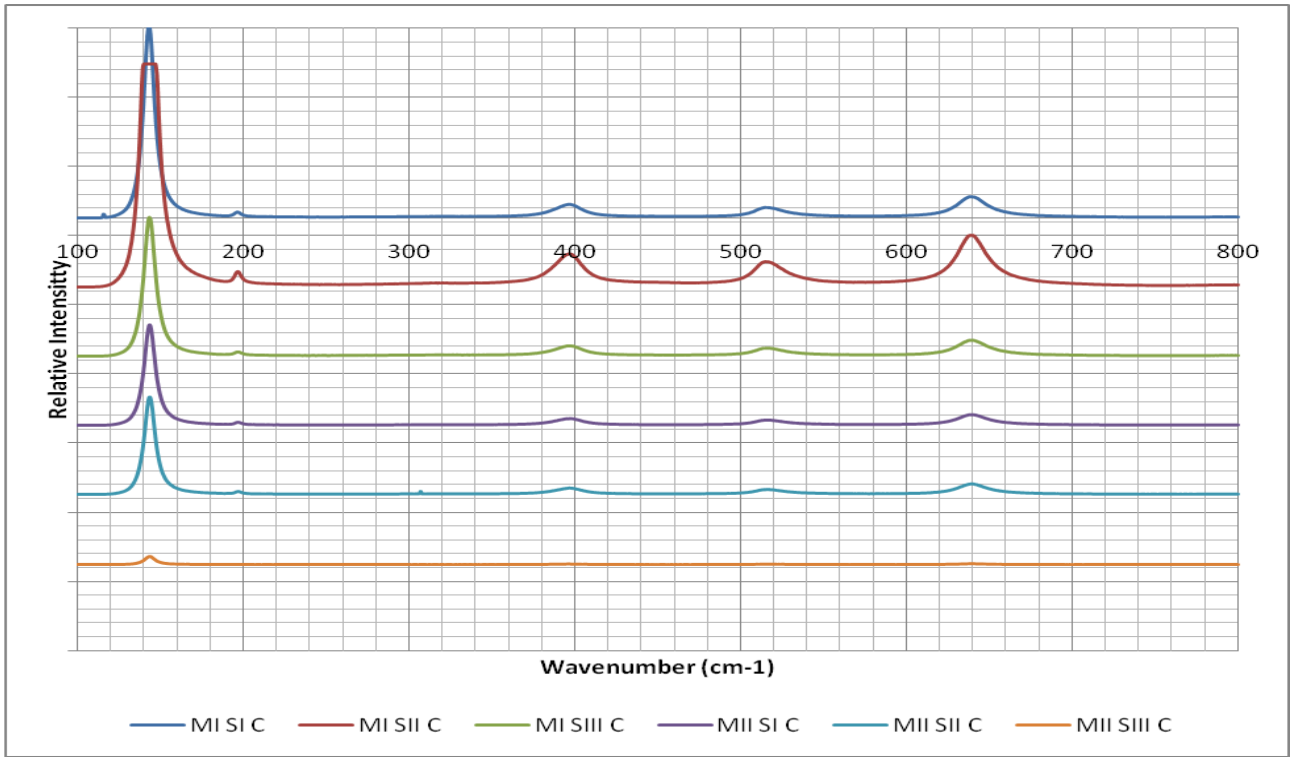

Figure 13: *Raman Spectroscopy data plot.*

Table 7: *Summary of data from Raman Spectroscopy*

Sample Name	Synthesis Method	Raw Material Composition (Zr:Ti)	Peak Point (wavenumber value)
MI SI C	Reflux	1:1	143.243, 196.216, 397.297, 514.595, 638.959
MI SII C	Reflux	1:0.5	140-147.027, 195.676,399.489, 516.216, 640
MI SIII C	Reflux	0.5:1	143.243, 192.297, 397.297, 513.513, 640
MII SI C	Impregnation	1:1	143.784, 196.757, 395.676, 515.135, 639.459
MII SII C	Impregnation	1:0.5	143.784, 196.757, 396.757, 514.054, 638.919
MII SIII C	Impregnation	0.5:1	144.324, 196.757, 395.135, 515.135, 631.919

4.1.3 X-ray Diffraction Results

The XRD patterns of 8 samples (S1, S2, S3, S4, S5, S6, S7, S10) show that most of sample are amorphous. It can be clearly observed that several stronger diffraction peaks assigned to the anatase phase of TiO_2, and a small diffraction peak at 30^o corresponding to the ZrO_2 tetragonal phase appear for all ZrO_2/TiO_2 samples. The pattern shown in **Figure 14** show that S1 to S6 fully crystallize at 600^oC. The XRD pattern of the samples match the JCPDS standard for $ZrTiO_4$ (Bhattacharya et al.). Observed reflections are compared with ICDD files for the compounds $ZrTiO_4$ (34-415); $Zr_5Ti_70_{24}$ (34-209); and Baddeleyte, the monoclinic ZrO_2 phase (37-1484). The intensity and width of peak vary with the Ti/Zr ratio, indicating that mesostructure is strongly affected by composition. By referring to the plot on the **Figure 14**, it is observed that the higher content of Zirconia leads to inhibition of crystallization due to lower crystallinity observed in the plot. In samples with higher content of zirconia, $ZrTiO_4$ and Baddeleyte reflection were observed. Heating treatment leads to crystallization to $ZrTiO_4$. The crystallization of the framework leads to the instantaneous phase transition and rapid nanocrystallite growth to $ZrTiO_4$ (Quan Yuan et al.). With the increase of ZrO_2 content, the diffraction peaks of TiO_2 become much weaker and wider gradually,

which means Sample 2 and Sample 5 with a smallest crystal size for TiO_2. This also indicates that the presence of the second component (ZrO_2) in sufficient amount notably inhibits the growth of TiO_2 nanocrystallites (Baochao, 2008).

Table 8 below shows the summary from XRD analysis. **Figure 14** shows the wide angle XRD pattern of samples calcined at 600^{o}C.

Table 8: *Summary of XRD analysis data.*

Sample	**1**	**2**	**3**	**4**	**5**	**6**
Space Group	Pnab (60)	Pnab (60)	Pnab (60)	Pnab (60)	Pnab (60)	Pnab (60)
Phase	$ZrTiO_4$	$ZrTiO_4$	$ZrTiO_4$	$ZrTiO_4$	$ZrTiO_4$	$ZrTiO_4$
Lattice Parameter (A)	TiO_2: a= 3.777 b= 3.77 c= 9.501 ZrO_2: a= 3.5984 b= 3.584 c= 5.152	TiO_2: a= 3.777 b= 3.77 c= 9.501 $ZrSc_2O_{13}$: a= 9.53 b= 9.53 c= 17.44	TiO_2: a= 3.777 b= 3.77 c= 9.501 $Zr_7O_{11}N_2$: a= 9.5759 b= 9.5769 c= 17.5913	TiO_2: a= 3.7845 b= 3.7845 c= 9.5145 $Zr(OH)_3(NO)_3$: a= 9.5759 b= 9.5769 c= 17.5913	TiO_2: a= 3.777 b= 3.777 c= 9.501 Baddeleyite: a= 5.3129 b= 5.2125 c= 5.1471	TiO_2: a= 3.777 b= 3.77 c= 9.501 $Zr_7O_{11}N_2$: a= 9.5759 b= 9.5769 c= 17.5913
Structure	ZrO_2: Tetragonal TiO_2: Anatase	$ZrSc_2O_{13}$: Hexagonal TiO_2: Anatase	$Zr_7O_{11}N_2$: Hexagonal TiO_2: Anatase	$Zr(OH)_3(NO)_3$: Monoclinic TiO_2: Anatase	Baddeleyite: Monoclinic TiO_2: Anatase	$Zr_7O_{11}N_2$: Hexagonal TiO_2: Anatase

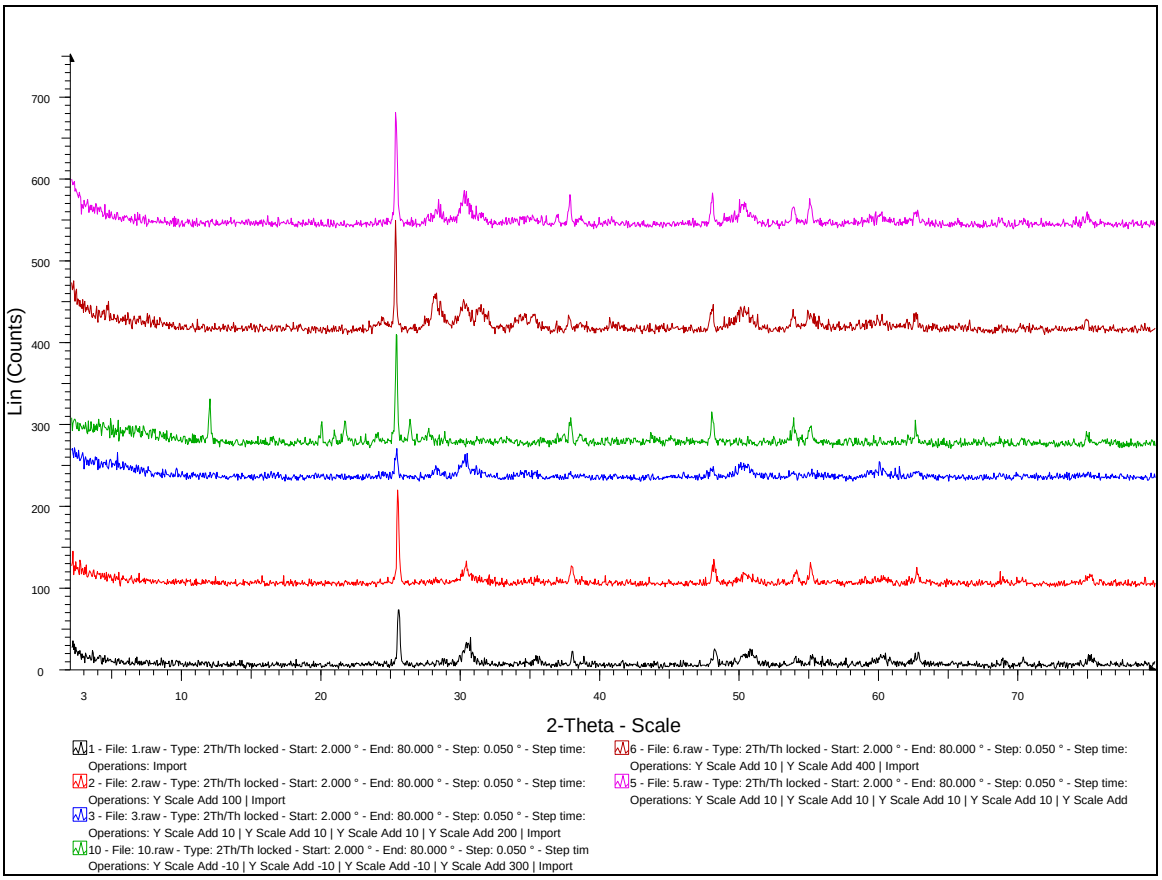

Figure 14: *Combination of XRD plot for samples done by reflux and impregnation*

4.1.4 Fourier Transform InfraRed result

FTIR analysis was used to determine the functional group of the synthesized samples. Refer to **Figure 15** and **16** for FTIR data plot.

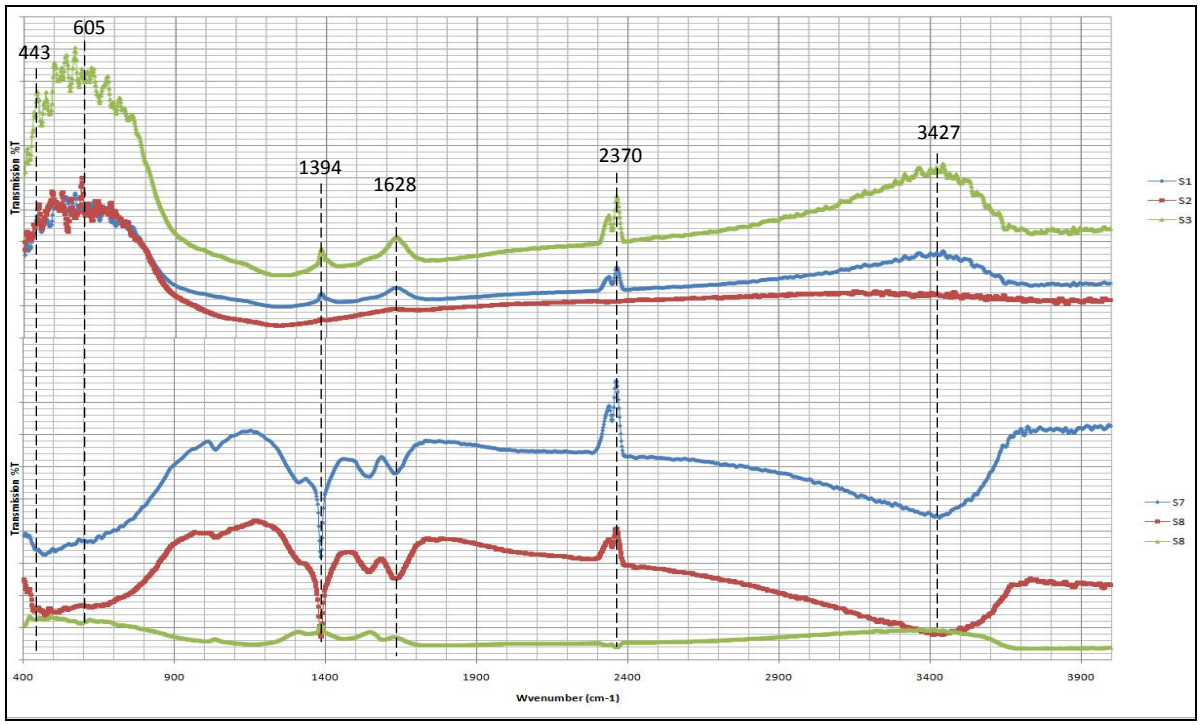

Figure 15: *FTIR plot for samples done by reflux synthesis.*

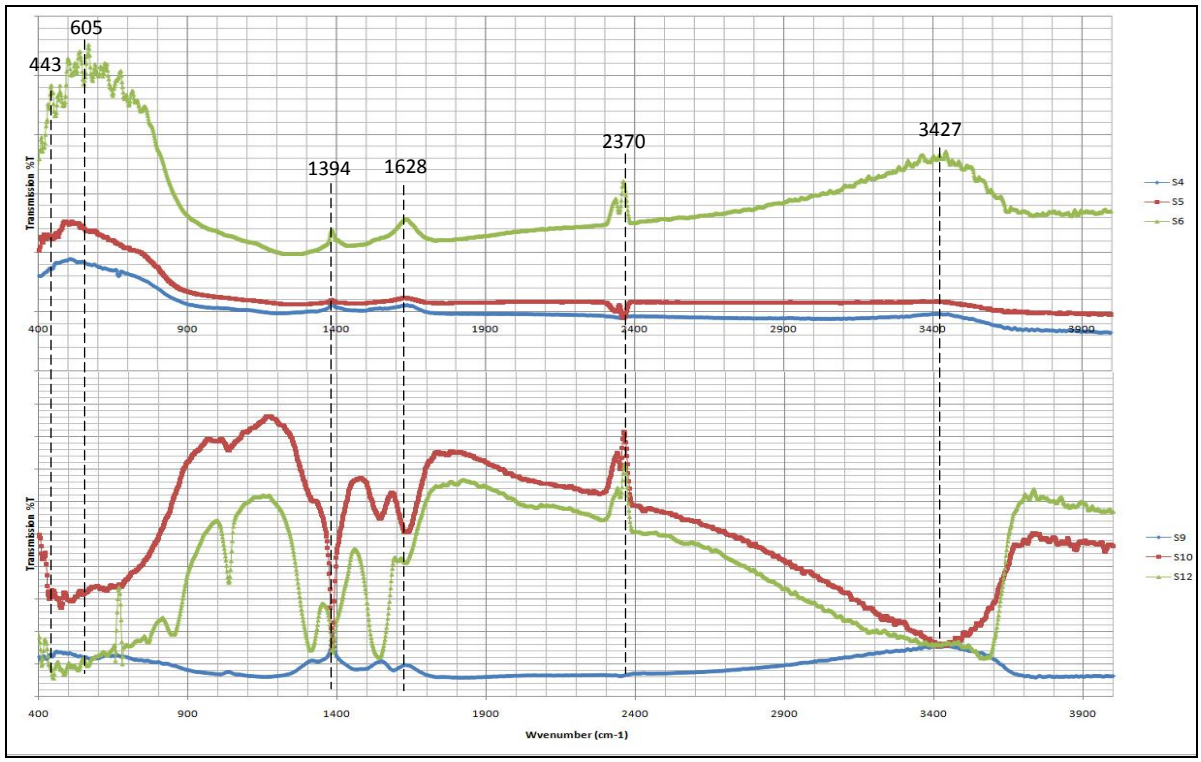

Figure 16: *FTIR plot for samples done by impregnation synthesis.*

The FTIR plot shows the comparison between calcined sample and uncalcined samples. Calcined samples are 1,2,3,7,8,9 while the others are uncalcined (**see Figure 15 & 16**). Based on **Figure 15** and **Figure 16**, it can be observed that absorption band at 443 cm^{-1}, which is almost the same with the study done by Jun et al (438cm^{-1}). The anatase band derived from the study was at 438 cm^{-1}. The absorption band at 605 cm^{-1} indicated the rutile phase band, which is close to study by Jun et al. (610cm^{-1}). It is observed that absorption at the range of 450-520 cm^{-1}, which is the characteristic of Zr-O bonds (Lopez et al.). The broad absorption band at 3410 cm^{-1} and characteristic peak at 1628 cm^{-1} are attributed to the O–H stretching and bending vibration respectively (Mishra et al.). The peak at 1394 cm^{-1} is clearly observed for all the samples calcined at 600 °C which can be assigned to the bending vibration mode of the N–H band. However, the N–H stretching is not marked due to the presence of broad O–H band in that region. The band at 2370 cm-^{1} appears to be due to the adsorbed dinitrogen resulting from the N,O decomposition (Lin et al.). Absorption at 3427cm^{-1} indicates hydroxyl group.

Samples 1,2,3,4,5,6 are the synthesis product which has been calcined while the Samples 7,8,9,10,11,12 are uncalcined products. By comparing the plot from the calcined and uncalcined products, it is observed that the calcined products shows lower intensity of transmittance that indicated reduction of hydroxyl group and N_2O group. The result is parallel from the estimation that there will be elimination of hydroxyl group and N_2O group. But the calcined products still give low transmittance of hydroxyl group and N_2O, indicating there are still residual of hydroxyl group and N_2O. This result can be related to the absorption of hydroxyl group from moistures into the samples and insufficient heat treatment to remove the N_2O.

CHAPTER 5

CONCLUSION & RECOMMENDATION

5.1 CONCLUSION

Both reflux and impregnation synthesis techniques successfully producing nanocrystalline $ZrTiO_4$. Both synthesis method is very simple; only requires the raw material to be mixed in deionized water to get the $ZrTiO_4$.

SEM result showed that with higher concentration of zirconia, the smaller are the grain size and more uniform is fractured surface and vice versa. The samples that has been calcined showed progressive reduction of porosity and grain size.

Based on the FTIR analysis, it was observed that there are reductions of hydroxyl and N_2O group in the calcined samples. Anatase TiO_2 characteristic was observed at 443 cm^{-1} while Zr-O in the range of 450-520 cm^{-1}.

Based on XRD and Raman Spectroscopy analysis, it showed that the characteristic of samples is highly affected by the composition of the samples. Samples with higher composition of Zirconia leads to inhibition of crystallization due to lower crystallinity observed in the plot. Sufficient amount of ZrO inhibit the growth of crystalline TiO_2 in the samples.

Based on the characterization done so far, samples with higher content of Zirconia is preferred due to reduction of pore size, smaller grain size and more uniform distribution. It also inhibits further growth of TiO_2 in the samples. Further characterization need to be done in order to get more information on the synthesized product.

5.2 RECOMMENDATION

Based on the experimental works done in the study, there are several key points that can be look into to improve the result of the study.

1) The sintering or the heat treatment should be done at higher temperature. It is observed that at 600^{o}C, there are still remaining N-H and hydroxyl group in the samples. Based on literature, the suitable temperature for the sintering is in the range of 800-1200^{o}C.
2) It is observed that there are still remaining hydroxyl group in the samples. It is hard to ignore the fact that the samples absorb moisture in the air. Careful preparation procedures can help to eliminate or reduce the absorption of hydroxyl group. For example by doing the procedure in vacuum space or regularly drying the samples. The characterization should be done immediately after the calcinations to prevent the moisture absorption.
3) High purity and homogeneity of ceramic material is essential for this study. Therefore, other synthesis methods are recommended to obtain pure ceramic product. Sol-gel synthesis method is one best method to obtain high purity ceramic. ZrTiO4 can be prepared by hydrolysis and condensation reaction of inorganic salts or alkoxides.
4) Further study need to done, especially on the effect of varies component composition and heat treatment. Both factors greatly affect the chemical and physical properties of the ceramic material.

REFERENCES

1. 1997, "Non-hydrolytic sol-gel process: zirconium titanate gels", *J. Mater. Chem.*, **7(2)**, pp. 279-284.
2. Bisquert, J., Cahen, D., Hodes, G., Rühle, S., Zaban, A. 2004, "Physical chemical principles of photovoltaic conversion with nanoparticulate, mesoporous dye-sensitized solar cells", *Journal of Physical Chemistry B*, **108**, pp. 8106-8118.
3. Cerqueira, M., Nasar, R.S., Leite, E.R., Longo, E., Varela, J.A. 1998, "Synthesis and characterization of PLZT (9/65/35) by the Pechini method and partial oxalate", *Materials Letters*, **35**, pp. 166–171.
4. Chen, D. et al. 1999. "Hydrothermal Synthesis and Characterization of Crystalline ZrxTi$_{1-x}$O4," *J. Mater. Sci*, **34**, 1379-1383.
5. Daturi, M., Cremona, A., Milella, F., Busca, G. and Vogna, E. 1997. "Characterisation of Zirconia - Titania Powders Prepared by Coprecipitation", *Journal of Be European Ceramic Society 18* (1998), pp. 1079-1087
6. Freitas, G.F.G., Nasar, R.S., Cerqueira, M., Melo, D.M.A, Longo, E., Varela, J.A. 2006, "Luminescence in semi-crystalline zirconium titanate doped with lanthanum", Materials *Science and Engineeering*, **A 434**, pp. 19-22.
7. Gao-Song Shao, Xue Jun Zhang, Zhong-Yong Juan. 2008. "Preparation and photocatalytic activity of hierarchically mesoporous-macroporous $TiO_{2-x}N_x$", *Applied Catalysis B: Environmental* **82**, pp. 208–218.
8. Górska, P., Zaleska, A., Kowalska, E., Klimczuk, T., Sobczak, J.W., Skwarek, E., Janusz, W. and Hupka, J. 2008. "TiO_2 photoactivity in vis and UV light: The influence of calcination temperature and surface properties", *Applied Catalysis B: Environmental*, **Volume 84**, Issues 3-4, 1 December 2008, Pages 440-447.
9. Gratze, M. and Durrant, J.R. 1912, "Dye sensitized mesoscopic solar cells", Giacomo Ciamician, 8th International Congress of Applied Chemistry,Washington and New York, September.
10. Grätzel, M. 2006, "Photovoltaic performance and long-term stability of dye-sensitized meosocopic solar cells", *C.R. Chimie* **9** pp. 578–583.

11. Kobasa, M., Kondrat'eva, I.V. 2006 "Effect of the composition of titanium-zirconium oxide system on their photocatalytic activity in the reduction of methylene blue by formaldehyde",*Theoretical and Experimental Chemistry*, **Vol. 42**, No. 6, pp. 352.
12. Kun-Mu Leea, Suryanarayanan, V., Kuo-Chuan Ho. 2007, "A study on the electron transport properties of TiO2 electrodes in dye-sensitized solar cells", *Solar Energy Materials & Solar Cells* **91**, pp. 1416–1420.
13. Kumara, G.R.A., Kaneko, S., Okuya, M., Tennakone, K. 2002, "Fabrication of dye-sensitized solar cells using triethylamine hydrothiocyanate as a CuI crystal growth inhibitor", *Langmuir* **18**, pp. 10493–10495.
14. Li, X.D., Zhang, D.W, Sun, Z., Chen, Y.W, Huang, S.M. "Metal-free indoline-dye-sensitized TiO_2 nanotube solar cells", Department of Physics, Engineering Research Center for Nanophotonics and Advanced Instrument, Ministry of Education, East China Normal University, North Zhongshan Rd. 3663, Shanghai 200062, PR China.
15. L. Lin, W. Lin, J.L. Xie, Y.X. Zhu, B.Y. Zhao and Y.C. Xie. 2007. **"**Photocatalytic properties of phosphor-doped titania nanoparticles", *Applied Catalysis B: Environmental*, **Vol 75**, Issues 1-2, 29 August 2007, Pages 52-58.
16. Macan, J., Markuš, S., Ivanković, H. "Preparation of zirconium titanate ceramics by sol-gel process", Faculty of Chemical Engineering and Technology, University of Zagreb HR-10001 Zagreb, Marulićev trg 19, p.p. 177.
17. Okada, K., Matsui, H., Kawashima, T., Ezyre, T., Tanabe, N., J. 2004, *Photochem. Photobiol*, **A 164** pp. 199.
18. O'Regan , B.; Grätze, M. Nature. 1991, 252, pp. 737.
19. Quan Yuan, Yang Liu, Le-Le Li, Zhen-Xing Li, Chen-Jie Fang, Wen-Tao Duan, Xing-Guo Li, Chun-Hua Yan. 2009. "Highly ordered mesoporous titania–zirconia photocatalyst for applicationsin degradation of rhodamine-B and hydrogen evolution", *Microporous and Mesoporous Materials* **124** pp. 169–178.
20. Vijayan, P., Mahendiran, C., Suresh, C., and Shanthi, K. 2009. *Catalysis Today*, **Vol. 141**, Issues 1-2, Pages 220-224.

21. Vittayakorn, N. 2006, “Synthesis and crystal structural study of microwave dielectric Zirconium Titanate powders via a mixed oxide synthesis route”, *Journal of Ceramic Processing Research*. **Vol. 7**, No. 4, pp. 288-291.
22. Voronsov, A. V., Altynnikov, A. A., Savinov, E. N. and Kurkin, E. N. 2001. **“**Correlation of TiO_2 photocatalytic activity and diffuse reflectance spectra”, Journal *of Photochemistry and Photobiology A: Chemistry*, **Vol. 144**, Issues 2-3, 7 November 2001, pp. 193-196.
23. Wong, M.S., Shih-Wei Hsu, Koteswara Rao, K. and Kumar, C.P. 2008. **“**Influence of crystallinity and carbon content on visible light photocatalysis of carbon doped titania thin films”, *Journal of Molecular Catalysis A: Chemical* **Vol. 279**, Issue 1, 2, pp. 20-26.
24. http://www.eifer.uni-karlsruhe.de/162.php
25. J. Macan, **A. Gajović[b] and H. Ivanković[a], “**Porous zirconium titanate ceramics synthesized by sol–gel process”, Journal of European Ceramic Society, Vol. 29, Issue 4, 691-696
26. F. Azough, R. Freer and J. Petzelt, A Raman spectral characterization of ceramics in the system ZrO_2–TiO_2, *J. Mater. Sci.* **28** (1993), pp. 2273–2276
27. P.R. de Lucena, E.R. Leite, F.M. Pontes, E. Longo, P.S. Pizani and J.A. Varela, Photoluminescence: a probe for short, medium and long-range self-organization order in $ZrTiO_4$ oxide, *J. Solid State Chem.* **179** (2006), pp. 3997–4002
28. Ussui, V., Lazar, D.R.R., Lima, N.B., Bressiani, A.H.A, Pachoal, J.O.A. “Zirconium Titanate: Synthesis and Processing of Fine Powders Prepared by Chemical Routes”,
29. Battacharya, A.K., Mallick, K.K., Hartridge, A., Woodhead, J.L. 1995. “Sol-gel preparation, structur and thermal stability of crystalline zirconium titanate microspheres”, Centre for Catalyric Systems and Materials Engineering, Department of Engineeering, University of Warwick, Coventry CV4 7AL, UK.
30. Lopez, T., Alvarez, M., Gomez, R. 2005. “ZrO_2 and Cu/ZrO_2 Sol-Gel Materials Spectroscopic Characterization”, *Journal of Sol-Gel Science and Technology 33*, 93-97.

31. Mishra, T., Hait, J., Aman, N., Gunjan, M., Mahato, B., Jana, R.K. 2008. "Surfactant mediated synthesis of spherical binary oxides photocatalytic with enhanced activity in visible light", *Journal of Colloid and Interface Science*, Vol. 327 Issue 2, pp 377-383.
32. Lin, J., Chen, H.Y., Chen, Tan, K.L., Zeng, H.B. 1996. "N_2O decomposition over ZrO_2 – an in-situ DRIFT, TPR, TPD and XPS study", *Applied Surface Science 103*, pp. 307-314.
33. Jun-Ying Zhang, et al. Nanocrystalline TiO2 films studied by optical, XRD and FTIR spectroscopy, *Journal of Non-Crystalline Solids*, 303 (2002) 134.

APPENDIX A

FTIR INTERPRETATION TABLE

APPENDIX B

FTIR RESULT

APPENDIX C

XRD RESULT

APPENDIX D

RAMAN SPECTROSCOPY RESULT

APPENDIX E

MATERIAL MSDS